Supporting Information for: Dynamical modes of sheared confined microscale matter

Sascha Gerloff* and Sabine H. L. Klapp†
Institut für Theoretische Physik, Hardenbergstr. 36, Technische Universität Berlin, D-10623 Berlin, Germany

Antonio Ortiz-Ambriz
Departament de Física de la Matèria Condensada, Universitat de Barcelona, Barcelona 08028, Spain and Institut de Nanociència i Nanotecnologia (IN2UB), Universitat de Barcelona, Barcelona 08028, Spain

Pietro Tierno
Departament de Física de la Matèria Condensada, Universitat de Barcelona, Barcelona 08028, Spain Institut de Nanociència i Nanotecnologia (IN2UB), Universitat de Barcelona, Barcelona 08028, Spain and Universitat de Barcelona Institute of Complex Systems (UBICS), Barcelona 08028, Spain

(Dated: September 3, 2020)

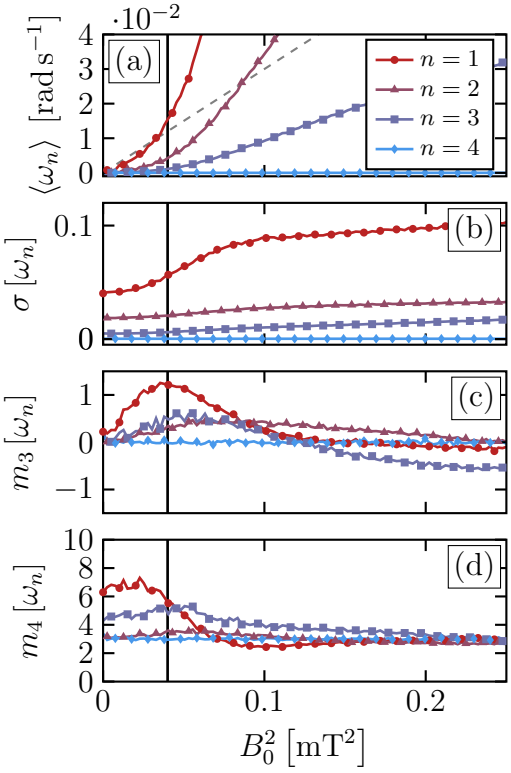

FIG. 1. Simulation results for the (a) mean-, (b) standard deviation, (c) skewness-, and (d) kurtosis of the angular velocity per ring. Figure (a) shows a closeup of the mean angular velocity plotted in Fig. 2(b) in the main text.

* s.gerloff@tu-berlin.de
† klapp@physik.tu-berlin.de

I. STOCHASTIC MOMENTS OF ω_n

The angular velocity distributions shown in Fig. 3 in the main text for the inner ring ($n = 1$) can be characterized by the corresponding stochastic moments, defined in Eqs. (8)-(10) in the main text, which we have plotted for all rings in Fig. 1. For better visualization of the depinning transition, we have plotted the mean $\langle\omega_n\rangle$ and standard deviation $\sigma[\omega_n]$ of the angular velocity in Fig. 1(a) and (b), corresponding to Fig. 2(b) and (d) in the main text. In Fig. 1(a) we have plotted $\langle\omega_n\rangle$ as function of the magnetic torque, emphasizing the depinning of the second and third layer ($n = 2, 3$). This depinning is clearly reflected by the higher stochastic moments, plotted in Fig. 1(c) and (d). In particular, we see a marked increase of the skewness ($m_3[\omega_n]$) as well as a steep decrease of the kurtosis ($m_4[\omega_n]$) of the inner ring ($n = 1$) at the critical torque $B^2_{0,c}$. Interestingly, the second and third layer display a slightly different response, including a negative skewness for large magnetic torques, as well as a maximum kurtosis at the critical torque. In the outer ring ($n = 4$) the angular velocity remains Gaussian distributed, i.e. $m_3 = 0$ and $m_4 = 3$, for all considered magnetic torques. The corresponding evolution of the distributions is shown in Fig 3(a) in the main text as well as Fig. 2(a)-(c), for the inner layer ($n = 1$) and the remaining layers, respectively. The angular velocity distributions of the second $P(\omega_2)$ and third layer $P(\omega_3)$ remain unimodal for all considered magnetic torques. However, they display asymmetric flanks which evolve with increasing magnetic torque, as already reflected by the skewness and kurtosis, see Fig. 1(c) and (d).

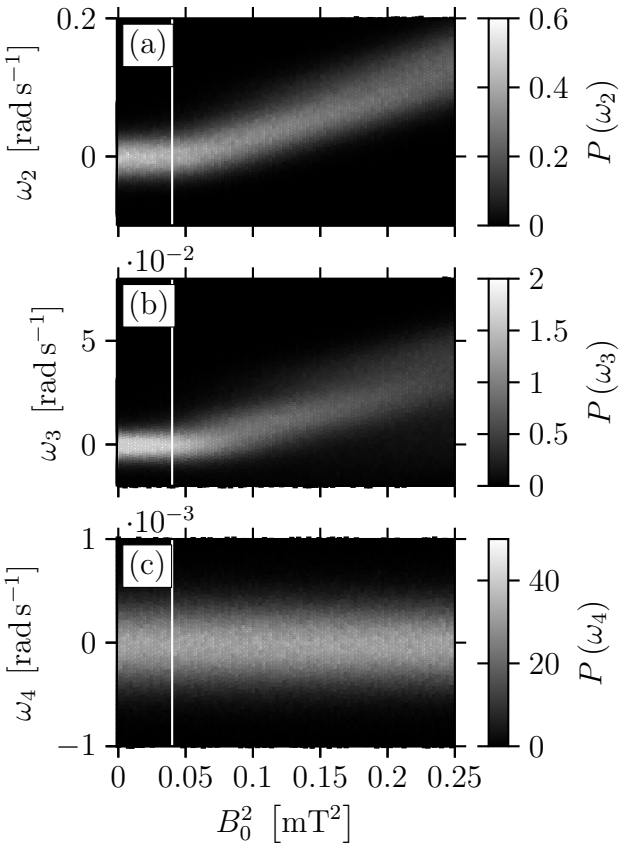

FIG. 2. Simulation results for the evolution of the distribution of the mean angular velocity of (a) the second ring ω_2, (b) the third ring ω_3, (c) the outer ring ω_4 during the magnetic field sweeps.

II. SHEAR STRESS FLUCTUATIONS

As discussed in the main text Sec. 6, the components of the stress tensor, i.e. the shear stress $\mathcal{S}_{r\varphi}$, the radial pressure $\mathcal{P}_r$ and the azimuthal pressure $\mathcal{P}_\varphi$, are fluctuating quantities, whose stochastic moments, as defined in the main text, clearly reflect the depinning transition at $B_{0,\mathrm{c}} = 0.04\,[\mathrm{mT}^2]$ clearly. In Fig. 3(a)-(l), we have plotted the corresponding stochastic moments, including the mean values (a)-(c) that where already reported in Fig. 8(a)-(c) in the main text. We find a marked response for the mean and standard deviation of all components of the stress tensor. In addition, the skewness of the shear stress displays a steep increase up to the critical magnetic torque, whereas the radial pressure displays a decrease of the skewness and kurtosis at $B_{0,\mathrm{c}}$. Note that the skewness and kurtosis of the azimuthal pressure as well as the kurtosis of the shear stress do not seem to reflect the transition.

III. WAITING AND JUMP TIMES DEFINITION

To calculate the jump and waiting times we follow a definition used for one-dimensional sinusoidal potentials, see Ref. [45] of the main text. The idea is to track the particle position relative to the location of the potential minima. A jump is initiated by passing a minimum either in positive or negative direction and concludes once the next minimum in this direction is passed. For the sheared colloidal system the potential minima correspond to the interstices of the next outer layer of particles, see Fig. 4. A forward jump is initiated by passing the current (S) interstice in positive azimuthal direction and concludes as soon as the particle passes the next interstice (F). Similarly, a backward jump is initiated by passing the current (S) interstice in negative azimuthal direction and concludes by passing the next interstice (B). The time between two jumps is defined as the waiting time.

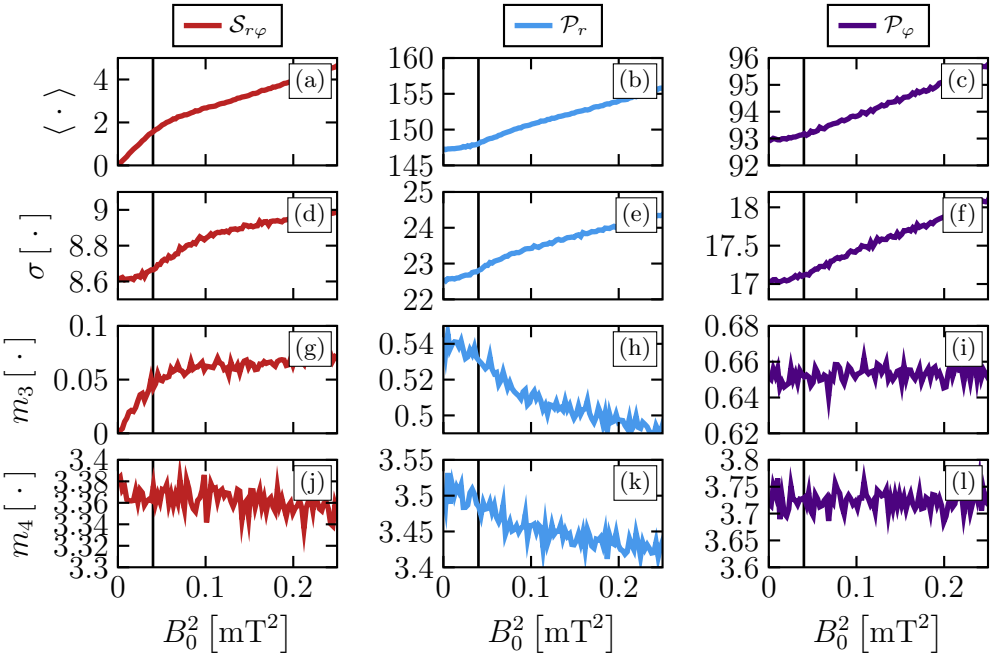

FIG. 3. (a)-(l) Simulation results for the stochastic moments of the shear stress and pressure components. (a)-(c) Mean as a function of magnetic torque B_0^2, (d)-(f) standard deviation as a function of B_0^2, (g)-(i) skewness as a function of B_0^2, and (j)-(l) kurtosis as a function of B_0^2. In all figures, the critical torque $B_{0,c}^2 = 0.04$ is emphasized by a solid black line.

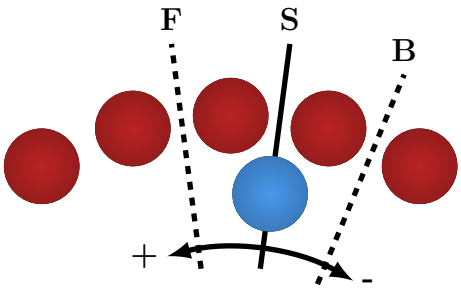

FIG. 4. Sketch for the waiting- and jump time definitions used in the main text. The red particles represent the outer neighboring particles of the blue particle. The three lines, solid and two dashed, represent the interstices, i.e. effective potential minima, accesible to the blue particle. They correspond to the start position (S), the forward jump target (F) and the backward jump target (B).